



Quantum control of electron spins in the two-dimensional electron gas of a CdTe quantum well with a pair of Raman-resonant phase-locked laser pulses

Timothy M. Sweeney, Carey Phelps, and Hailin Wang*

Department of Physics, University of Oregon, Eugene, OR 97403, USA

(Received 27 April 2011; published 10 August 2011)

We demonstrated optical spin control of a two-dimensional electron gas in a modulation-doped CdTe quantum well by driving a spin-flip Raman transition with a pair of phase-locked laser pulses. In contrast to single-pulse optical spin control, which features a fixed spin-rotation axis, manipulation of the initial relative phase of the pulse pair enables us to control the axis of the optical spin rotation. We show that the Raman pulse pair acts like an effective microwave field, mapping the relative optical phase onto the phase of the electron spin polarization and making possible ultrafast, all-optical, and full quantum control of the electron spins.

DOI: [10.1103/PhysRevB.84.075321](https://doi.org/10.1103/PhysRevB.84.075321)

PACS number(s): 78.67.De, 42.50.Ex, 42.50.Md, 71.35.Pq

I. INTRODUCTION

Full quantum control of individual electron spins and spin ensembles is important for spin-based quantum information processing. Full quantum control can be achieved by driving the transition between the two spin states with a microwave pulse, as demonstrated in gate-defined quantum dots (QDs) fabricated from a two-dimensional electron gas (2DEG).^{1,2} Quantum control of electron spins can also be realized via coherent optical interactions. Optical spin control can take advantage of ultrafast laser technologies to enable spin rotations in a picosecond timescale. Coherent optical interactions can also be exploited for the generation of spin-photon quantum entanglement in atomic as well as solid-state spin systems.³⁻⁶ Optical spin control using ultrafast laser pulses has been demonstrated in various semiconductor systems⁷⁻¹³ and also in trapped ions.¹⁴ In these experiments, individual off-resonant laser pulses act like an effective direct current (DC) magnetic field along the optical axis, inducing a spin rotation about the fixed axis. Full quantum control of spins, however, requires spin rotation about two orthogonal axes.¹⁵ For spin rotations about an axis orthogonal to the optical axis, recent studies have exploited spin precession about an external magnetic field^{9,12} and have also attempted the use of additional laser pulses to induce a geometrical phase shift.^{16,17}

An all-optical approach to achieve full quantum control of electron spins involves driving a spin-flip Raman transition with a pair of Raman-resonant and phase-locked laser pulses that are detuned from the respective dipole optical transitions.¹⁸ Here, we report the first experimental demonstration of this approach using a 2DEG in a modulation-doped CdTe quantum well (QW). In comparison with single-pulse optical spin control, a Raman pulse pair acts like an effective microwave pulse with a phase given by the relative optical phase of the pulse pair. By manipulating the initial relative phase of the pulse pair with an optical pulse-shaping technique, we are able to control the axis of optical spin rotation. We show that the phase-locked pulse pair maps the relative optical phase directly onto the phase of the electron spin polarization, enabling all-optical, full quantum control of the electron spins. The experimental results, including Rabi oscillations of electron spins in the 2DEG, are well described by a theoretical analysis based on optical Bloch equations (OBEs).

Among various semiconductor spin systems, optical spin control in 2DEGs is especially challenging. 2DEGs do not feature atomic-like, spectrally sharp optical transitions. In addition to the rapid dipole decoherence, coherent optical processes in 2DEGs are also complicated by inherent manybody interactions. The successful experimental demonstration of the Raman pulse pair approach in a 2DEG indicates the feasibility of extending the all-optical spin control to systems, such as gate-defined QDs, that do not feature atomic-like optical transitions.

II. PHYSICAL MECHANISMS OF OPTICAL SPIN ROTATION

The basic physical mechanism of optical spin rotations and the difference between the Raman pulse pair approach and the single-pulse approach can be elucidated by an effective Hamiltonian for spin-flip Raman transitions. Figure 1(a) shows two spin states, $|+\rangle$ and $|-\rangle$, with frequency separation ω_B , coupling to an excited state, $|e\rangle$, via two dipole optical transitions. The two transitions feature the same polarization selection rule such that an individual optical pulse can couple to both dipole transitions. In the limit that the excited state dynamics adiabatically follow the external optical fields as well as the dynamics of the two spin states, the three-level system can be reduced to a two-level spin system driven by effective magnetic fields.¹⁸ The effective Hamiltonian of the two-level system after the adiabatic elimination of the excited state dynamics is given by:

$$H_{\text{eff}} = \frac{\hbar\omega_B}{2}\sigma_z - \hbar\Omega_R \cos(\delta t + \varphi)\sigma_x - \frac{\mu^2(E_1^2 + E_2^2)}{4\hbar\Delta}\sigma_x, \quad (1)$$

where the two incident optical fields feature nearly equal amplitudes, E_1 and E_2 , a frequency difference of δ , and an initial relative phase of ϕ . Δ is the average detuning of the optical fields from the dipole transitions [see Fig. 1(a)], and $\Omega_R = \mu^2 E_1 E_2 / (2\hbar^2 \Delta)$ is the effective Rabi frequency for the spin-flip Raman transition. For simplicity, we assume that the two dipole transitions have the same dipole matrix element, μ .

Optical spin rotations can be understood in terms of the effects of effective DC and alternating current (AC) magnetic fields. The third term in Eq. (1) results from individual laser pulses. This term corresponds to spin rotations induced by a

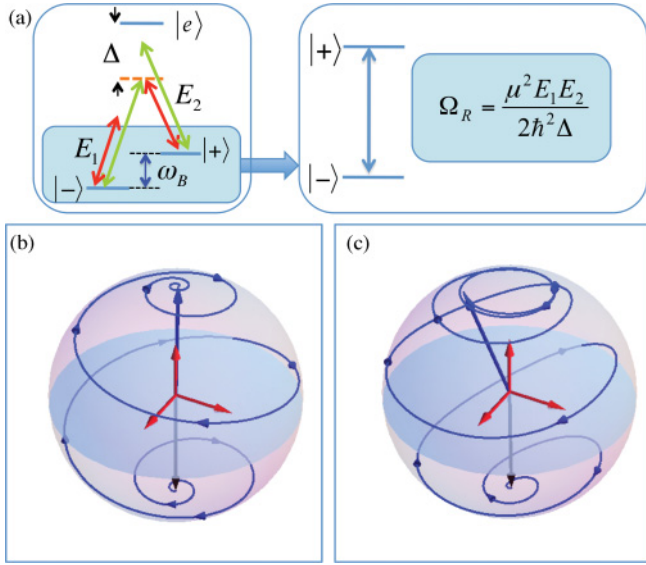


FIG. 1. (Color online) (a) A three-level system interacting with a Raman pulse pair and the equivalent effective two-level spin system under the adiabatic approximation. (b) and (c) Trajectory of a Bloch spin vector initially along the $-z$ -axis driven by a Raman pulse pair with $\theta = \pi$. The trajectory is calculated with the effective two-level Hamiltonian in Eq. (1). Effects of the effective DC magnetic field are included in (c), but not in (b).

DC magnetic field along the x -axis, as extensively investigated in earlier studies.^{7–14} The second term in Eq. (1) results from the Raman pulse pair. This term corresponds to spin-rotations induced by an AC magnetic field or, equivalently, a microwave with a phase given by the relative optical phase of the Raman pulse pair. As shown in Eq. (1), the resonance condition for the spin-flip Raman transition is $|\delta| = \omega_B$. Spectrally sharp

spin-flip Raman resonances have been observed in frequency-domain coherent Raman experiments in GaAs QWs^{19,20} and also in CdTe QWs.²¹ Note that for a Λ -type three-level system, where the two dipole transitions have orthogonal polarization selection rules, the effective AC magnetic field remains nearly the same as in Eq. (1) (see the Appendix).

III. EXPERIMENTAL RESULTS

The sample used in our studies consists of 10 periods of 10 nm CdTe wells and 45 nm $\text{Cd}_{0.84}\text{Zn}_{0.16}\text{Te}$ barriers.²² The modulation doping density is estimated to be $3 \times 10^{10} \text{ cm}^{-2}$. In the presence of an in-plane external magnetic field (the Voigt geometry), a three-level system as shown in Fig. 1(a) can be formed in the 2DEG, with the excited state being a trion state, for which an exciton is bound to an electron.²² As illustrated in Fig. 2(a), we define the direction of the external magnetic field as the z -axis and the normal of the QW plane as the x -axis. For our experimental studies, $\sigma+$ circularly polarized Raman pulse pairs couple the two electron spin states to a trion state that contains a heavy-hole with $J_x = 3/2$ and two electrons with opposite spins, as shown schematically in Fig. 2(a). At low temperature, the trions in the CdTe QW sample feature an absorption line width of 1.6 meV (0.8 nm) and a binding energy of 2.5 meV (1.25 nm), as shown in Fig. 2(b). Experimental studies presented here were all carried out at $T = 5 \text{ K}$ and $B = 5 \text{ T}$ in a superconducting magnetic cryostat, unless otherwise specified. Under these conditions, $k_B T / (\hbar \omega_B) = 0.8$, leading to a small but net spin polarization along the z -axis, which we use for the experimental demonstration of optical spin control. Note that in addition to the Voigt geometry, a three-level system involving the two electron spin states can also be formed for the light-hole transitions in the Faraday geometry, for which the external magnetic field is normal to the QW plane.^{23,24}

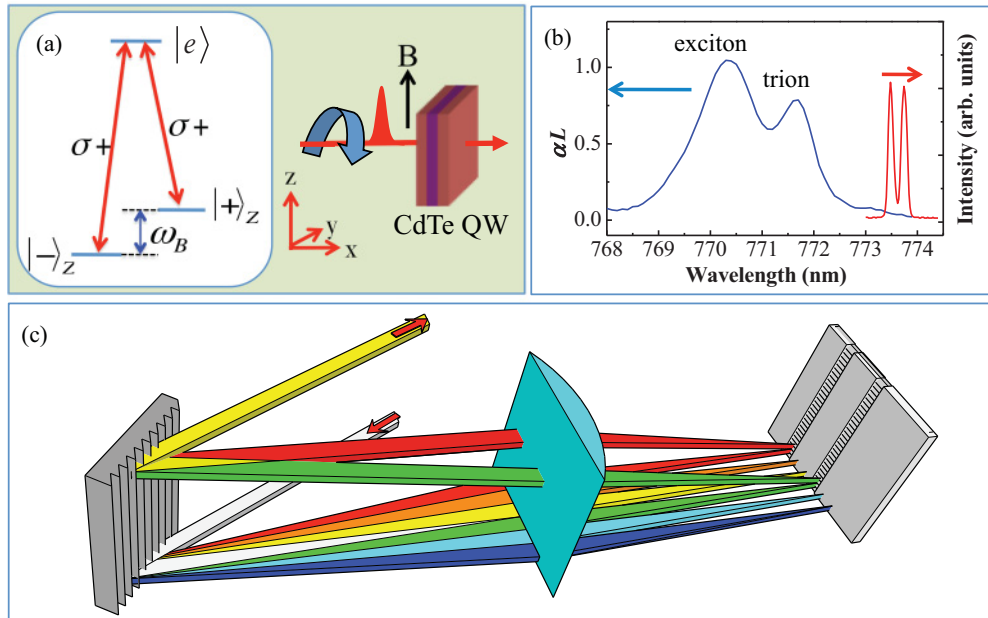


FIG. 2. (Color online) (a) Experimental geometry and schematic of the three-level system used, as discussed in the text. (b) Exciton and trion absorption spectrum at 5 K, along with the spectrum of a Raman pulse pair. (c) Schematic illustrating the use of a grating-based optical pulse shaper and a spatial light modulator to generate phase-locked Raman pulse pairs.

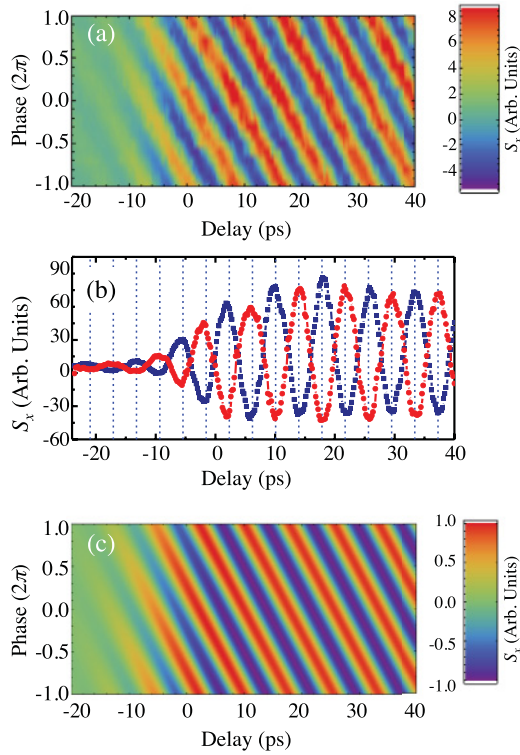


FIG. 3. (Color online) (a) Spin polarization projected along the x -axis as a function of the delay between the probe and the Raman pulse pair, as the initial relative phase, ϕ , of the pulse pair is stepped incrementally from -2π to 2π . (b) The spin beats obtained with a π phase difference in ϕ are π out of phase. (c) Theoretically calculated spin polarization projected along the x -axis, with ϕ varied from -2π to 2π .

We used optical pulse shaping to generate phased-locked pulse pairs. As shown schematically in Fig. 2(c), the output from a picosecond mode-locked Ti:Sapphire laser with a repetition rate of 80 MHz is sent through a grating-based optical pulse shaper. For our experimental setup, a 2200 line/mm grating, a cylindrical lens with a focal length of 1m, and a phase-only liquid-crystal spatial light modulator (LCSLM) from Holoeye, Inc., are used. The LCSLM diffracts two components of the input spectrum toward the top of the diffraction grating. The rest of the spectrum is terminated at a beam stop (not shown in the diagram). The two diffracted spectral components are then collimated and combined by the lens and the diffraction grating into a single output beam. The initial phase difference of the two pulses in the pulse pair is set by the optical path length of one pulse relative to the other. The spectral width, spectral separation, intensity, and relative phase of the two optical pulses can all be controlled with the programmable LCSLM. Figure 2(b) shows the spectrum of a Raman pulse pair used in the spin rotation experiment. The two laser pulses feature nearly the same intensity and a spectral width of 0.1 nm (corresponding to a duration of approximately 15 ps). The spectral separation of the two pulses (0.25 nm or 0.5 meV) is set to match the spin splitting. The spot size of the Raman pulse pair on the sample is estimated to be $5 \times 10^{-5} \text{ cm}^2$. The two pulses in the pulse pair travel through nearly identical paths, avoiding relative phase fluctuations

in the propagation process. Note that off-resonant spectrally shaped laser pulses, instead of phase-locked pulse pairs, have been used in an earlier study to manipulate electron spins in CdTe QWs.²⁵

We used the Raman pulse pair to directly excite the electron spin system. Figure 3(a) shows the dynamics of S_x , the electron spin polarization projected along the x -axis, as the initial relative phase of the pulse pair, ϕ , is stepped from -2π to 2π . For this experiment, Raman pulse pairs with θ near $\pi/2$ were detuned 1 nm below the trion resonance. The projection of the electron spin polarization along the x -axis (the growth axis) was measured via differential transmission with a probe pulse that is 2 ps in duration and is resonant with the trion transition. The change in the transmission of the probe induced by the precessing spin polarization was detected with a lock-in amplifier as a function of the delay between the probe and the center of the Raman pulse pair. The spectral line width of the circularly polarized probe pulse is much greater than the electron Zeeman splitting, enabling the measurement of the electron spin polarization projected along the x -axis.

The spin dynamics in Fig. 3(a) feature a Larmor spin precession about the external magnetic field with a period of 8 ps, corresponding to an electron spin splitting of 0.5 meV. As shown in Fig. 3(a), the phase of the spin beats varies linearly with ϕ , while the amplitude of the spin beats remains independent of ϕ . Figure 3(b) highlights two traces of the spin beats, which are π out of phase for a π phase difference in ϕ .

Figures 4(a) and 4(b) show the dynamics of S_x as a function of the average power of the Raman pulse pair, with a fixed initial relative phase, obtained at a detuning of $\Delta = 1.05 \text{ nm}$ and 1.7 nm , respectively. Figure 4(c) plots the amplitude of the spin beats for the fourth period of the spin beats (counting from the center of the Raman pulse pair) as a function of the average power obtained at three different detunings. The power dependence of the beat amplitude shows damped Rabi oscillations of the electron spins. In Fig. 4(c), the average power is normalized to the detuning, demonstrating that the effective pulse area associated with the Rabi oscillation is inversely proportional to the detuning. Note that optical excitations of trions or excitons in a 2DEG can lead to a large increase in the spin as well as dipole decoherence rates.^{26,27} As shown in Fig. 4(c), the fidelity of the optical spin rotation deteriorates with increasing optical power, and especially when the Raman pulse pair is tuned close to the trion resonance. The fidelity can be further improved with greater detuning from respective dipole transitions and with the use of longer laser pulses.

IV. DISCUSSION

For a detailed theoretical analysis, we used the OBEs for the three-level system without the adiabatic approximation, where experimentally determined parameters including dipole and spin decoherence times (1 ps and 0.5 ns, respectively), spin splitting, effective pulse area, and pulse duration are used. For simplicity, effects of inhomogeneous broadening are not included. Figure 3(c) plots the calculated S_x as a function of time, as ϕ is varied from -2π to 2π . The calculated spin dynamics agree well with those in Fig. 3(a). Theoretically, the effective AC magnetic field, which is equivalent to a

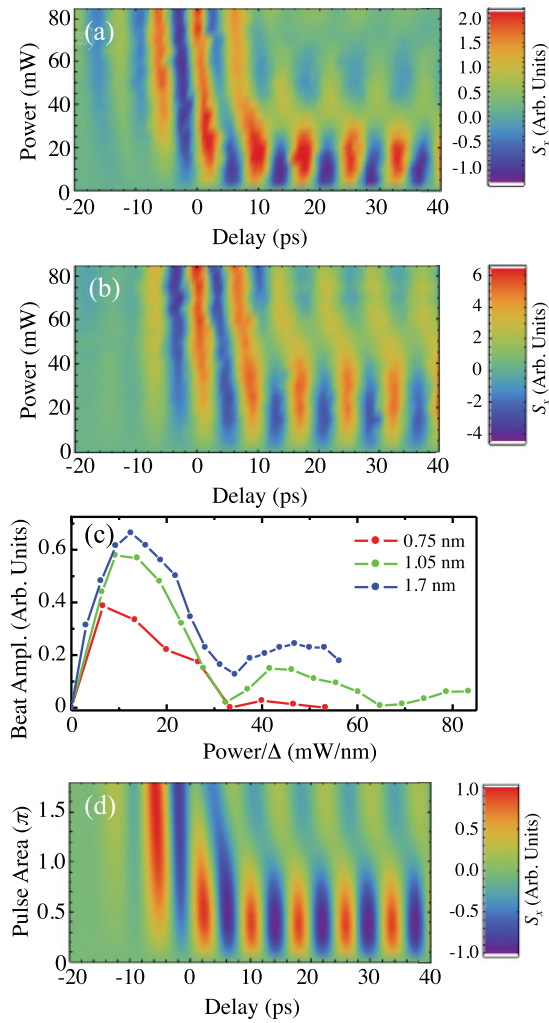


FIG. 4. (Color online) (a) and (b) Spin polarization projected along the x -axis as a function of the delay between the probe and the Raman pulse pair, with increasing average power for the Raman pulse pair and with $\Delta = 1.05$ nm for (a) and 1.7 nm for (b). (c) The amplitude of the spin beats for the fourth period as a function of the average power of the Raman pulse pair normalized to the detuning, with the detuning indicated in the figure. (d) Theoretically calculated spin polarization projected along the x -axis, with increasing effective pulse area.

microwave with its phase given by the relative optical phase, induces a spin polarization in the x - y plane characterized by the density matrix element,

$$\rho_{+-}(t) \propto \Delta N \exp[-i(\omega_B t + \varphi)], \quad (2)$$

where ΔN is the initial population difference between the two spin states. The dependence of the spin-beat phase on ϕ shown in Fig. 3(a) demonstrates that the phase-locked pulse pair maps the relative optical phase onto the phase of the electron spin polarization, as expected from Eq. (2).

The mapping between the relative optical phase and the spin beat phase as shown in Fig. 3(a) is a direct manifestation showing that the relative optical phase controls the axis of optical spin rotation. Within the rotating-wave approximation (RWA) for the spin-flip transition, the spin rotation induced

by a microwave is governed by the Bloch equation in the precessing frame of the electron spins (effects of decay processes are not included), $d\mathbf{s}/dt = \mathbf{s} \times \mathbf{\Omega}$, where \mathbf{s} is the Bloch vector for the electron spins in the precessing frame, and $\mathbf{\Omega} = (\Omega_R \cos \phi, \Omega_R \sin \phi, 0)$, which determines both the axis and rate of the spin rotation. A microwave pulse induces a spin rotation about an axis along $(\cos \phi, \sin \phi, 0)$, with a rotation angle given by the effective pulse area $\theta = \int \Omega_R(t) dt$. In this case, a spin flip from $|-\rangle$ to $|+\rangle$ corresponds to a π spin rotation about an axis set by the initial relative optical phase, along with spin precession about the z -axis, as shown in Fig. 1(b). In general, for a spin polarization initially along the z -axis, a microwave pulse induces a spin polarization in the x - y plane by rotating or tipping the polarization away from the z -axis. The phase of the induced polarization in the x - y plane is determined by ϕ and the subsequent spin precession process, as indicated in Eq. (2).

Spin rotations induced by a Raman pulse pair are also influenced by the effective DC magnetic field that results from individual laser pulses. In the absence of the DC magnetic field, a Raman pulse pair with $\theta = \pi$ rotates a Bloch vector initially along the $-z$ axis to the $+z$ -axis, at which spin precession stops. Figure 4(b), however, shows that as θ goes through π , the spin beat amplitude does not vanish, and furthermore the phase of the spin beats varies gradually instead of flipping by π . Note that these behaviors are not as prominent in Fig. 4(a) due to the degradation of the spin-rotation fidelity at the relatively small detuning. The non-vanishing spin beats and the gradual phase variation of the spin beats near $\theta = \pi$ are caused by the DC magnetic field. To illustrate these effects, we show in Fig. 1(c) a calculated trajectory of a Bloch vector initially along the $-z$ axis driven by a Raman pulse pair with $\theta = \pi$. The calculation includes both the effective DC and AC fields in Eq. (1), but it does not include effects of spin decoherence. The DC field induces a spin rotation about the x -axis in the non-precessing frame. As a result, the Bloch vector remains slightly away from the z -axis and continues to precess after the passage of the π pulse. Figure 4(d) shows the calculated S_x as a function of time, as θ is varied from 0 to beyond 1.5π , for which the OBEs for the three-level system were used. The calculated spin dynamics reproduce all key features of the experimental results in Fig. 4(b).

Note that the effective DC magnetic field does not lead to decoherence and therefore does not degrade the fidelity of the optical spin rotation. The effects of single-pulse spin rotations can be compensated with a proper choice of two Raman pulse pairs. In the limit that the electron spin splitting far exceeds both the spin decoherence rate and the spectral width of individual pulses in the pulse pair, effects of single-pulse spin rotation become negligible.

Optical spin control with Raman pulse pairs can overcome inherent limitations of the single-pulse approach. As discussed earlier, Raman pulse pairs can enable all-optical, arbitrary spin rotation. Perhaps equally important, the Raman pulse pair approach can function with relatively long laser pulses, while the efficient operation of the single-pulse approach requires the use of laser pulses that have a short duration compared with the spin precession period. For spin systems such as 2DEGs or gate-defined QDs that do not feature atomic-like optical transitions, the use of relatively long laser pulses in optical spin

control is crucial in order to avoid strong optical excitations that can lead to excessive dipole decoherence. In addition, the ability to programmably manipulate Raman pulse pairs with spectral pulse shaping also makes it possible to optimize the spin rotation process with feedback control.²⁸

V. CONCLUSION

In conclusion, we have successfully demonstrated the optical control of electron spins in a 2DEG by driving a spin-flip Raman transition with a pair of phase-locked laser pulses. In comparison with the single-pulse approach, a phase-locked Raman pulse pair behaves effectively like a microwave pulse, with a phase given by the relative optical phase, mapping the relative optical phase onto the phase of the electron spin polarization. The Raman pulse pair approach can overcome inherent limitations of the single-pulse approach, opening up an avenue for ultrafast, all-optical, full quantum control of electron spins and potentially extending optical spin control to systems such as gate-defined QDs that do not feature atomic-like optical transitions.

ACKNOWLEDGMENTS

This work has been supported by the National Science Foundation under Grant No. 0804559 and by ARL-ONAMI. We thank Ronald Cox for providing the CdTe QW sample used in our experiments.

APPENDIX

Here, the effective two-level Hamiltonian for spin-flip Raman transitions is presented.

1. Introduction

Here, we derive the effective two-level Hamiltonian for a spin-flip Raman transition in the limit of adiabatic approximation. For the three-system shown in Fig. A1, the two spin states couple to the common excited state via two dipole optical transitions. The Hamiltonian for this three-level system interacting with two external optical fields can be written in the form:

$$H = \begin{pmatrix} \hbar\omega_e & V_+ & V_- \\ V_+^* & \hbar\omega_B/2 & 0 \\ V_-^* & 0 & -\hbar\omega_B/2 \end{pmatrix}, \quad (\text{A1})$$

where V_+ and V_- are the matrix elements for the relevant dipole optical interactions. No assumptions are made at this point with respect to the polarization selection rule of the dipole transition. In the rotating frame, the state vector of the three-level system can be written as

$$|\psi(t)\rangle = C_e \exp(-i\bar{\omega}t)|e\rangle + C_+|+\rangle + C_-|-\rangle, \quad (\text{A2})$$

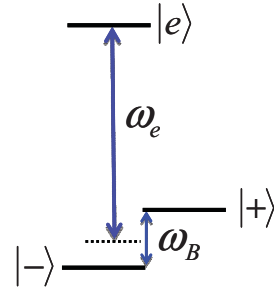


FIG. A1. Schematic of a three-level system where the two lower spin states couple to the common excited state via two dipole optical transitions.

where $\bar{\omega} = (\omega_1 + \omega_2)/2$ is the average frequency of the two external optical field. Within the rotating wave approximation, the Schrödinger equation for the state vector is given by

$$i\hbar \frac{d}{dt} \begin{pmatrix} C_e \\ C_+ \\ C_- \end{pmatrix} = \hbar \begin{pmatrix} \Delta & \Omega_+ & \Omega_- \\ \Omega_+^* & \omega_B/2 & 0 \\ \Omega_-^* & 0 & -\omega_B/2 \end{pmatrix} \begin{pmatrix} C_e \\ C_+ \\ C_- \end{pmatrix}, \quad (\text{A3})$$

where $\Delta = \omega_e - \bar{\omega}$ is the average detuning for the dipole transition, and we define $V_+ = \hbar\Omega_+ \exp(-i\bar{\omega}t)$ and $V_- = \hbar\Omega_- \exp(-i\bar{\omega}t)$.

For sufficiently large Δ , the dynamics of the excited state follow adiabatically the external optical fields as well as the dynamics of the two lower-level spin states. Decoherence related to the excited state can also become negligible. In this adiabatic limit, we have

$$i \frac{d}{dt} C_e = \Delta C_e + \Omega_+ C_+ + \Omega_- C_- \approx 0. \quad (\text{A4})$$

The three-level system can then be reduced effectively to a two-level system,

$$i\hbar \frac{d}{dt} \begin{pmatrix} C_+ \\ C_- \end{pmatrix} = H_{\text{eff}} \begin{pmatrix} C_+ \\ C_- \end{pmatrix}, \quad (\text{A5})$$

with an effective Hamiltonian given by

$$H_{\text{eff}} = \hbar \begin{pmatrix} \frac{\omega_B}{2} - \frac{|\Omega_+|^2}{\Delta} & -\frac{\Omega_+^* \Omega_-}{\Delta} \\ -\frac{\Omega_+ \Omega_-^*}{\Delta} & -\frac{\omega_B}{2} - \frac{|\Omega_-|^2}{\Delta} \end{pmatrix}, \quad (\text{A6})$$

where $|\Omega_+|^2/\Delta$ is the optical Stark shift induced by the external fields.

2. Three-level system with orthogonal polarization selection rules

For three-level systems where the two dipole transitions have orthogonal polarization selection rules, two optical fields, with amplitude E_1 and E_2 and frequency ω_1 and ω_2 , couple to two separate dipole transitions, respectively. In this case, we have

$$\begin{aligned} \Omega_+ &= \frac{\mu_+ E_1}{2\hbar} \exp\left(-i\frac{\delta t}{2} - i\phi\right), \\ \Omega_- &= \frac{\mu_- E_2}{2\hbar} \exp\left(-i\frac{\delta t}{2}\right), \end{aligned} \quad (\text{A7})$$

where μ_+ and μ_- are the respective dipole matrix elements (assumed to be real), ϕ is the initial phase difference between the two optical fields, and $\delta = \omega_1 - \omega_2$. The effective two-level Hamiltonian is now given by

$$H_{\text{eff}} = \hbar \begin{pmatrix} \frac{\omega_B}{2} - \frac{|\Omega_+|^2}{\Delta} & -\frac{\Omega_R}{2} \exp[i(\delta t + \phi)] \\ -\frac{\Omega_R}{2} \exp[-i(\delta t + \phi)] & -\frac{\omega_B}{2} - \frac{|\Omega_-|^2}{\Delta} \end{pmatrix}, \quad (\text{A8})$$

where $\Omega_R = \mu_+ \mu_- E_1 E_2 / (2\hbar^2 \Delta)$ is the effective Rabi frequency for the spin-flip Raman transition. In the limit of equal optical Stark shifts for the two spin states, the two optical fields are equivalent to a microwave field with the phase determined by the relative phase of the two optical fields.

3. Three-level system with same polarization selection rules

For three-level systems where the two dipole transitions have the same polarization selection rules, each optical field couples to both dipole transitions. In this case, we have

$$\Omega_+ = -\frac{\mu_+}{2\hbar} \left[E_1 \exp\left(\frac{\delta t}{2} - i\phi\right) + E_2 \exp\left(i\frac{\delta t}{2}\right) \right] \quad (\text{A9a})$$

and

$$\Omega_- = -\frac{\mu_-}{2\hbar} \left[E_1 \exp\left(-i\frac{\delta t}{2} - i\phi\right) + E_2 \exp\left(i\frac{\delta t}{2}\right) \right]. \quad (\text{A9b})$$

The effective two-level Hamiltonian is now given by

$$H_{\text{eff}} = \hbar \begin{pmatrix} \frac{\omega_B}{2} - \frac{|\Omega_+|^2}{\Delta} & -\Omega_R \cos(\delta t + \phi) \\ -\Omega_R \cos(\delta t + \phi) & -\frac{\omega_B}{2} - \frac{|\Omega_-|^2}{\Delta} \end{pmatrix} + \begin{pmatrix} 0 & -\frac{\mu_+ \mu_-}{4\hbar^2 \Delta} (E_1^2 + E_2^2) \\ -\frac{\mu_+ \mu_-}{4\hbar^2 \Delta} (E_1^2 + E_2^2) & 0 \end{pmatrix}. \quad (\text{A10})$$

The second term in the Hamiltonian is due to the effects of individual optical fields and corresponds effectively to a DC magnetic field, leading to single-pulse spin rotation about the optical axis.

In the limit that $|\delta| \approx \omega_B$, $\mu_+ \approx \mu_-$, and ω_B is large compared with both the spectral bandwidth of the individual laser pulse and the spin decoherence rate, the effects of the individual laser fields become negligible, and the two external fields are equivalent to a microwave field with the phase determined by the relative optical phase of the two optical fields, as is the case for three-level systems with orthogonal polarization selection rules.

*Corresponding author: hailin@uoregon.edu

¹F. H. L. Koppens, C. Buizert, K. J. Tielrooij, I. T. Vink, K. C. Nowack, T. Meunier, L. P. Kouwenhoven, and L. M. K. Vandersypen, *Nature* **442**, 766 (2006).

²K. C. Nowack, F. H. L. Koppens, Y. V. Nazarov, and L. M. K. Vandersypen, *Science* **318**, 1430 (2007).

³B. B. Blinov, D. L. Moehring, L. M. Duan, and C. Monroe, *Nature* **428**, 153 (2004).

⁴D. Matsukevich, T. Chaneliere, M. Bhattacharya, S. Lan, S. Jenkins, T. Kennedy, and A. Kuzmich, *Phys. Rev. Lett.* **95**, 040405 (2005).

⁵J. F. Sherson, H. Krauter, R. K. Olsson, B. Julsgaard, K. Hammerer, I. Cirac, and E. S. Polzik, *Nature* **443**, 557 (2006).

⁶E. Togan, Y. Chu, A. S. Trifonov, L. Jiang, J. Maze, L. Childress, M. V. G. Dutt, A. S. Sorensen, P. R. Hemmer, A. S. Zibrov, M. D. Lukin, *Nature* **466**, 730 (2010).

⁷J. A. Gupta, R. Knobel, N. Samarth, and D. D. Awschalom, *Science* **292**, 2458 (2001).

⁸S. G. Carter, Z. Chen, and S. T. Cundiff, *Phys. Rev. B* **76**, 201308 (2007).

⁹D. Press, T. D. Ladd, B. Y. Zhang, and Y. Yamamoto, *Nature* **456**, 218 (2008).

¹⁰J. Berezovsky, M. H. Mikkelsen, N. G. Stoltz, L. A. Coldren, and D. D. Awschalom, *Science* **320**, 349 (2008).

¹¹K. M. C. Fu, S. M. Clark, C. Santori, C. R. Stanley, M. C. Holland, and Y. Yamamoto, *Nature Physics* **4**, 780 (2008).

¹²A. Grelich, S. E. Economou, S. Spatzek, D. R. Yakovlev, D. Reuter, A. D. Wieck, T. L. Reinecke, and M. Bayer, *Nature Physics* **5**, 262 (2009).

¹³C. Phelps, T. Sweeney, R. T. Cox, and H. L. Wang, *Phys. Rev. Lett.* **102**, 237402 (2009).

¹⁴W. C. Campbell, J. Mizrahi, Q. Quraishi, C. Senko, D. Hayes, D. Hucul, D. N. Matsukevich, P. Maunz, and C. Monroe, *Phys. Rev. Lett.* **105**, 090502 (2010).

¹⁵A. Barenco, C. H. Bennett, R. Cleve, D. P. Divincenzo, N. Margolus, P. Shor, T. Sleator, J. A. Smolin, and H. Weinfurter, *Phys. Rev. A* **52**, 3457 (1995).

¹⁶S. E. Economou and T. L. Reinecke, *Phys. Rev. Lett.* **99**, 217401 (2007).

¹⁷E. D. Kim, K. Truex, X. D. Xu, B. Sun, D. G. Steel, A. S. Bracker, D. Gammon, and L. J. Sham, *Phys. Rev. Lett.* **104**, 167401 (2010).

¹⁸P. C. Chen, C. Piermarocchi, L. J. Sham, D. Gammon, and D. G. Steel, *Phys. Rev. B* **69**, 075320 (2004).

¹⁹S. O'Leary, H. Wang, and J. Prineas, *Opt. Lett.* **32**, 569 (2007).

²⁰P. Palinginis and H. Wang, *Phys. Rev. B* **70**, 153307 (2004).

²¹S. O'Leary and H. Wang (unpublished).

²²K. Kheng, R. T. Cox, Y. M. Daubigne, F. Bassani, K. Saminadayar, and S. Tatarenko, *Phys. Rev. Lett.* **71**, 1752 (1993).

²³S. Sarkar, P. Palinginis, P. Ku, C. Chang-Hasnain, N. Kwong, R. Binder, and H. Wang, *Phys. Rev. B* **72**, 035343 (2005).

²⁴S. Crankshaw, F. G. Sedgwick, M. Moewe, C. Chang-Hasnain, H. L. Wang, and S. L. Chuang, *Phys. Rev. Lett.* **102**, 206604 (2009).

²⁵J. H. Versluis, A. V. Kimel, V. N. Gridnev, D. R. Yakovlev, G. Karczewski, T. Wojtowicz, J. Kossut, A. Kirilyuk, and T. Rasing, *Phys. Rev. B* **80**, 235326 (2009).

²⁶E. A. Zhukov, D. R. Yakovlev, M. Bayer, M. M. Glazov, E. L. Ivchenko, G. Karczewski, T. Wojtowicz, and J. Kossut, *Phys. Rev. B* **76**, 205310 (2007).

²⁷S. O'Leary and H. L. Wang, *Phys. Rev. B* **77**, 165309 (2008).

²⁸S. E. Economou, L. J. Sham, Y. W. Wu, and D. G. Steel, *Phys. Rev. B* **74**, 205415 (2006).